

Experimental and numerical study on the hysteretic behavior of composite partially restrained steel frame-reinforced concrete infill walls with vertical slits

Guohua Sun¹ · Qiang Gu¹ · Qicai Li¹ · Youzhen Fang¹

Received: 10 May 2017 / Accepted: 5 October 2017 / Published online: 14 October 2017
© Springer Science+Business Media B.V. 2017

Abstract The work presented in this study aimed to investigate the hysteretic behavior of composite partially restrained (PR) steel frame-reinforced concrete infill walls (PSRCW) with vertical slits, which consisted of a PR steel frame, a slit-reinforced concrete (RC) infill wall, and shear connectors. An experimental program at one-third scale of a one-bay by three-story PSRCW with vertical slits was tested under horizontal cyclic loading. The seismic behavior was examined in terms of the lateral load-carrying capacity, ductility, deformability, lateral stiffness, and energy dissipation. The results showed that this kind of structure exhibited superior ductility and deformability, as well as excellent energy-dissipation capacity. The slit RC infill walls exhibited flexure-dominated behavior and significantly increased the lateral load-carrying capacity. In contrast, the slit RC infill walls decreased the rotation demand on the PR connections from earthquake, which avoided the fracture failure of the beam-to-column connection. Additionally, the test results were verified, and relative parametric analyses of PSRCW with vertical slits were conducted by using a simplified macro fiber model to illustrate the factors that influence the structural hysteretic behavior.

Keywords Steel frame · PR connections · Slits · Infill walls · Cyclic test · Fiber model

1 Introduction

A steel frame with reinforced concrete infill walls (SRCW) mainly consists of a steel frame as a boundary and RC infill walls. According to early research, the SRCW can be divided into two categories (Liau and Kwan 1983): (1) integral infill frames that employ shear connectors along the interfaces between the steel frame and the RC infill wall and (2) non-

✉ Guohua Sun
sungh-529@163.com

¹ School of Civil Engineering, Suzhou University of Science and Technology, Suzhou 215011, China

integral infill frames without any shear connectors between two parts. In the SRCW system, the surrounding steel frame is used to sustain gravity loads and the overturning moment from earthquake or wind, while the RC infill wall serves as a shear-dominated panel to resist lateral shear. The important action of shear connectors along the interface between the steel frame and the RC infill walls was first realized by Mallick and Severn (1968) based on a number of half-cyclic dynamic loading tests on small-scale infilled steel frames. Their test results revealed that the employment of shear connectors in the loading corners could prevent the rotation of the RC infill walls and increase the lateral stiffness of test specimens. Liauw and Kwan (1985) conducted a series of static, dynamic, and cyclic tests on both integral and non-integral infill steel frames with RC infill walls. The test results verified that the presence of shear connectors along the entire interface between the steel frame and the RC infill walls significantly increased both the lateral strength and stiffness of the SRCW system. In Japan, two sets of these tests were carried out to investigate the seismic behavior of a steel frame with RC infill walls subjected to the combined action of constant gravity loading and static cyclic lateral loading (Makino 1985). A few headed studs were used to prevent the out-of-plane failure of the RC infill walls, and the orientation and section of steel column were investigated. It was found that the infilled steel frame with columns bent about their strong axis exhibited more favorable deformation capacity. The deterioration of the lateral strength of the infilled steel frame with a stocky-rolled wide flange section was slower than that of the strength of infilled steel frame with thin-walled wide flange section. To enhance the rotation capacity of the beam-to-column connection, a cyclic loading test on one-third-scale steel-frame structures with composite RC infill walls and PR connections was carried out at the University of Minnesota (Tong 2001; Hajjar 2002; Tong et al. 2005). The test results showed that this composite structure had the potential to offer enough lateral strength to resist the forces from earthquakes and lateral stiffness to control drift for low- to moderate height buildings located in earthquake-prone regions. A total of three lateral-load transferring paths were obtained, including shear stud-infill interaction, steel frame-infill strut interaction, and deformation of the steel frame. The headed studs sustained approximately 80–90% of the total lateral load at the design level of lateral force and the remaining 10–20% was resisted by the compression strut. However, the majority of the headed studs placed along the beam-infill interface failed due to low-cycle fatigue fracture, which resulted in poor ductility of the SRCW structure. Therefore, Tong et al. noted that reducing the post-peak strength degradation is necessary for further research. Peng and Gu (2013) performed a test of a two-story, one-bay steel frame with RC infill walls and PR connections under cyclic loading. The low-cycle fatigue failure of the head studs at the interface between the top steel beam and the RC infill wall also occurred. Sun et al. (2011) developed an innovative RC infill wall, i.e., a concealed-vertical-slit RC infill wall, and conducted a test at one-third-scale, one-bay two-story PR steel frame with concealed vertical slit RC infill walls (PSRCW) under cyclic loading. The test results showed that the PSRCW structure exhibited the obvious two-stage mechanical features. Before the concealed vertical slits were crushed (corresponding to the first stage), the RC infill wall deformed as a whole shear panel which could provide considerably large initial lateral stiffness and sufficient lateral strength. After the concealed vertical slits were crushed (corresponding to the second stage) the height-to-width ratio of the RC infill wall increased significantly. As a result, the RC infill wall deformed as a series of flexural columns that could provide considerable deformation capacity.

To enhance the structural deformability, some researchers attempted to use the ordinary reinforced concrete panel, high-performance fiber-reinforced concrete or lightweight infill

walls to retrofit the steel frame (Wu et al. 2016, Cao et al. 2017; Olsen and Billington 2011; Lignos et al. 2014; Hou et al. 2016). Otherwise, the ductile concrete-filled steel tubular columns were also adopted in the SRCW system (Liao et al. 2009, 2012, Wang et al. 2017). In addition, to further improve the ductility of the RC infill wall, some researchers proposed modifying the slit RC infill walls by introducing the penetrated slits into a solid RC infill wall. The purpose was to increase the height-to-width ratio of the RC infill walls. The slit RC infill wall served as a ductile lateral resisting element that can be traced to studies by Omori et al. (1966) in Japan. The slit RC infill wall behaves as many parallel flexural columns to sustain wind or earthquake, which can undergo considerably large flexural deformations relative to the shear deformation. Lian and Zou (1996) performed an experimental study on six specimens without a surrounding steel frame under cyclic loading, and the ductile failure mode of the slit RC wall was observed. Zhao et al. (2012) conducted cyclic tests on two one-bay, two-story, and one-third-scale steel frames with a prefabricated slit RC infill wall. The lateral strength, ductility, stiffness degradation, and energy dissipation of test specimens were investigated. Both specimens possessed considerably excellent deformability, and exhibited beyond a 2% inter-story drift ratio. The global ductility of SRCW structure can be further enhanced by optimizing the surrounding PR steel frame. The evolutionary computation techniques for optimum design of planar PR steel frames proposed by Sánchez-Olivares and Tomás (2013) can be used to design the SRCW structure.

In general, some previous experimental studies that have been conducted do not consider the influence of the surrounding steel frame. In addition, the boundary restraint condition of the test specimen might not be reflected reasonably. Part of the test specimens used small-scale models with an unreasonable steel profile for single-story frames. The latter could not reflect the influence of an overturning moment or the complex interaction between the steel frame and the RC infill walls. In addition, several studies on the PSRCW structure still adopted solid RC infill walls that deformed as the entire shear panel and resulted in unexpected poor deformability and ductility. Therefore, the slit RC infill wall, which behaved as a series of separate flexural columns, has been suggested for employment in the PSRCW structure. This type of seismic-resistant element has been proposed since (1966) by Omori et al., which could provide fairly ductile behavior as well as stable cyclic performance by changing the shear behavior into flexural behavior for the RC infill wall. However, research on the seismic behavior of PSRCW with vertical slits is rare, except for two one-third scale one-bay, two-story specimens tested under cyclic lateral loading (Zhao et al. 2012). Therefore, in the present study, a three-story, one-bay PSRCW with vertical slits sub-assembly at one-third scale has been experimentally investigated under cyclic lateral loading, and a more reasonable boundary condition is reflected by adopting the top and bottom half-story solid RC infill walls to a certain extent. The simplified macro fiber model has been used to simulate the hysteretic behavior and compare with the test results. Parametric studies, such as the type of beam-to-column connection, height-to-width ratio of slit wall, concrete strength and steel-bar ratio, are also performed to evaluate the sensitivity of the predicted hysteretic behavior to design parameters of slit RC infill wall using the macro model.

2 Experimental program

2.1 Test specimen

A three-story, one-bay PSRCW with vertical slits at one-third scale was designed and fabricated. The test specimen, labeled S-SLW, was 1500 mm wide measured between boundary frame member centerlines. The height of the second story was 1200 mm, and that of the first and third stories was 600 mm, equal to one-half of the second story. The solid RC infill wall with a thickness of 100 mm was adopted in the first and third story to avoid serious damage or crush prior to the second story. The slit RC infill wall was only used in the second story, and the thickness was 80 mm. The main objective of using two half-stories was to reflect the boundary restriction action on the intermediate steel beam. The steel beams and columns were made of grade Q235B according to the Chinese standard ($f_y = 235 \text{ N/mm}^2$). Steel columns were $\text{H}150 \times 150 \times 7 \times 10 \text{ mm}$ [H-overall depth (d) \times flange width (b_f) \times web thickness (t_w) \times flange thickness (t_f)]. The top beam was $\text{H}150 \times 150 \times 7 \times 10 \text{ mm}$, and the intermediate and bottom beams were $\text{H}150 \times 100 \times 6 \times 9 \text{ mm}$. The size and configuration of specimen S-SLW are shown in Fig. 1.

The dimension of the slit wall was 735 mm (height) \times 245 mm (width) \times 80 mm (thickness), and the height-to-width ratio was 3. The details of the second-story slit RC infill wall are shown in Fig. 2. Six plain bars were used as longitudinal reinforcement in each slit wall (the longitudinal reinforcement ratio was equal to 0.87%). The stirrup was fabricated using 4 mm plain bars, which were spaced at 50 mm in the middle zone and 30 mm in both end zones. The reinforcement details of the slit wall are shown in Fig. 3a. The width of the boundary element in both the slit and solid RC infill walls was 135 mm,

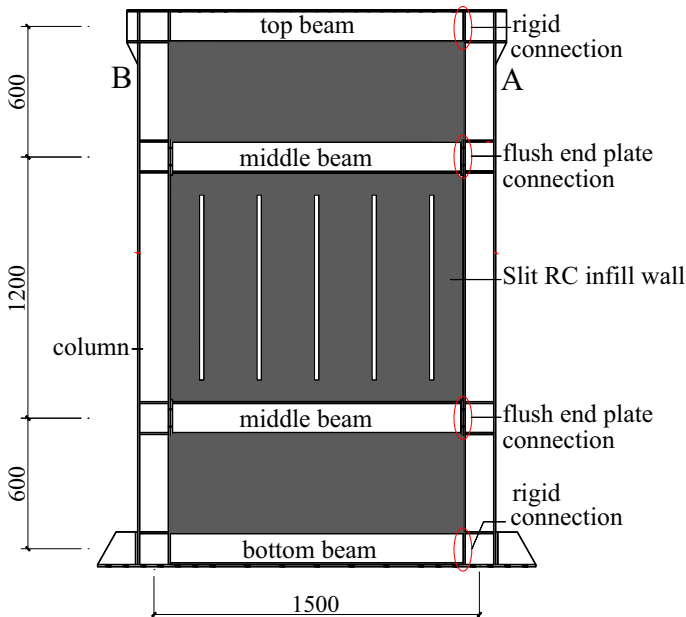


Fig. 1 The dimensions of the S-SLW sub-assembly

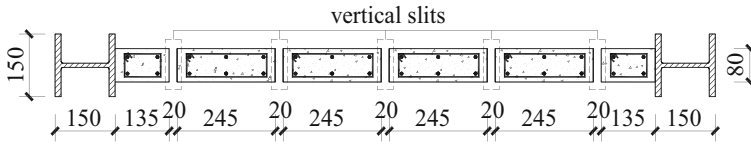


Fig. 2 Details of the slit RC infill wall

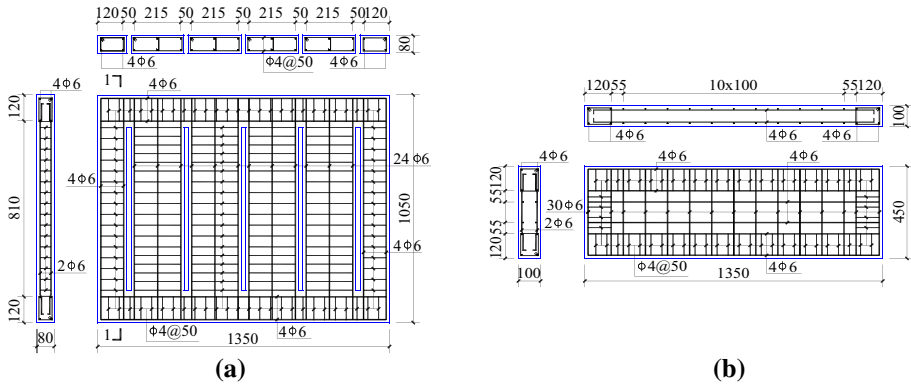


Fig. 3 Reinforcement details of the RC infill wall: **a** slit RC infill wall; **b** solid RC infill wall

and four 6 mm plain bars were used as longitudinal reinforcement, corresponding to a 1.05% longitudinal reinforcement ratio. The stirrup of 4 mm plain bars was spaced at 50 mm along the whole boundary element. In addition, the first-story and third-story solid RC infill walls contained an arrangement of two layers of 6 mm plain bars spaced at 120 mm. The reinforcement details of the solid RC infill wall are shown in Fig. 3b. All of the steel bars used in the slit RC infill walls were made of Grade HPB235 with a specified yield stress of 235 N/mm².

A flush end plate connection was employed to enhance the rotation capacity of the beam-to-column connections in specimen S-SLW. The dimensions of the end plate were 10 mm (thickness) × 120 mm (width) × 160 mm (height). A steel beam was connected to the column flange by means of flush end plate connections with four high-strength bolts (M16, grade 10.9, yield stress f_y of 960 N/mm², ultimate stress f_u of 1040 N/mm²). The plastic moment capacity of the PR connections considering the effect of the axial force was approximately 50% of that of the steel beam. The details of the flush end plate connection are illustrated in Fig. 4.

For the transfer of the inner force between the surrounding steel frame and the RC infill walls, channel connectors were adopted. These were welded and spaced at 100 mm intervals along the frame-wall interface. The boundary-reinforcing cages were used as an effective method to avoid or delay primary failure around the shear connectors due to the limited thickness of the RC infill wall. The details of the channel connector are shown in Fig. 5.

Two steel coupons were tested for each material, and the average results of the coupon tests for the material used in the current specimen are shown in Table 1. The average compressive strength of the concrete used in RC infill wall was 33.12 N/mm², from a 150 mm × 150 mm × 150 mm cube taken on the test day.

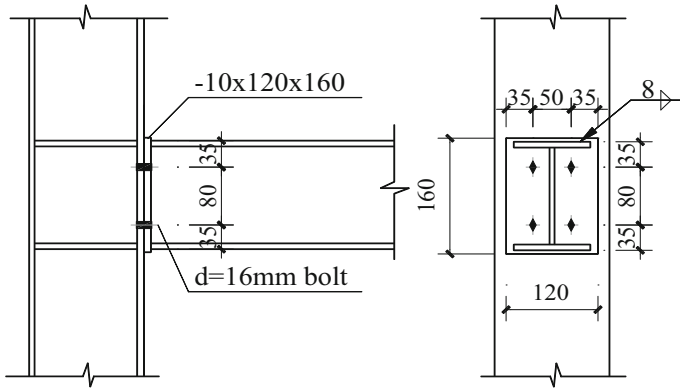


Fig. 4 Details of flush end plate connection

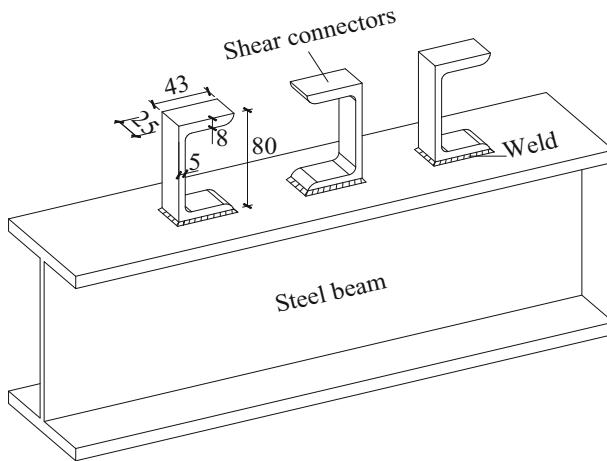


Fig. 5 Details of the channel connector

Table 1 Material properties of Steel

Steel	Yield stress f_y (N/mm ²)	Ultimate stress f_u (N/mm ²)	Elongation at rupture (ϵ_u /%)
Column flange	258.16	417.24	30.28
Column web	268.32	409.61	31.00
Beam flange	301.43	452.86	26.36
Beam web	304.54	461.91	32.36
End plate	262.82	412.85	28.17
D4-plain bar	–	457.82	11.25
D6-plain bar	385.14	542.31	26.15

2.2 Test setup and instrumentation

The test setup for specimen S-SLW is shown in Fig. 6. The main components of the test setup are the actuator, top loading beam, bottom reaction beam, press beam, mechanical jack, and lateral bracings. During the test, a cyclic lateral load or displacement was applied by the actuator to the top of the specimen through a loading beam. The lateral shear and overturning moment were transferred to laboratory ground by the bottom reaction beam, pressing beam and mechanical jack. To prevent an out-of-plane movement of the test specimen, the lateral braces were designed and provided at the end of the loading beam.

Four linear variable displacement transducers (LVDT) were equipped to monitor the global displacement (L1-L4), including all the story drifts (Fig. 6). In addition, a set of LVDTs was installed on the test specimen for measuring local deformations. Some important data such as the slit RC infill wall deformation (L5-L6), slippage between the beam-wall interface (L7-L8), PR rotation (L9-L16) and separation between the column-wall interface (L17-L21) were also measured. Strain gages were mounted at some critical locations of the test specimen, such as column flanges and webs, PR connections, and shear connectors to obtain the local strain deformation.

2.3 Loading protocol

The cyclic loading protocol was modified and adopted according to the SAC protocol (1997) for consideration of the deformation characteristics of the PSRCW with vertical slits. First, load control was applied including one cycle at 50, 100, and 200 kN, when the specimen was almost in the elastic range. After that, the control was switched to displacement control that included three cycles at a total drift ratio of ± 0.50 , ± 0.75 , ± 1.00 , ± 1.25 , ± 1.50 , ± 1.75 , $\pm 2.00\%$ and so on, until the test specimen failed.

3 Discussion of test results

3.1 Crack pattern and failure mode

At the load control stage During the 50 kN level, the flexural cracks occurred almost simultaneously at both ends of some of the slit walls, oriented approximately at $\pm 30^\circ$ to

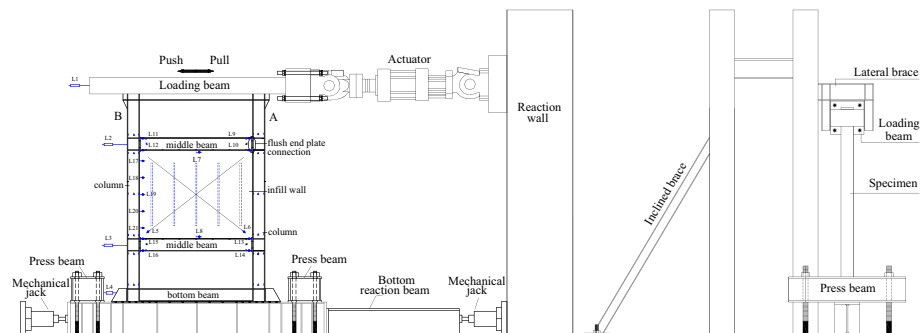


Fig. 6 Test setup

the horizontal line. These cracks originated from the corner of the slit wall, and the length of the cracks was approximately 120 mm. During the 100 kN level, some new flexural cracks continued to occur in the slit walls. Note that flexural cracks appeared along two different directions at the ends of all the slit walls due to the cyclic loading. In this phase of the loading process, some short hairline cracks were also detected. The test specimen still remained elastic, and the hysteretic loop was small and symmetric. During the 200 kN level, more cracks developed inside all of the RC infill walls, and different types of cracks were observed, including horizontal flexural and inclined shear cracks. These original flexural cracks located at the ends of the slit walls and extended across the entire slit walls. Some new cracks gradually occurred at the inner region of the slit walls. The width of the crack was approximately 1 mm. Some inclined shear cracks were observed in the first- and third-story solid RC infill walls, and the inclinations of these shear cracks were approximately 45° . The first- and third-story solid RC infill walls started to develop an obvious “X” shape in the distribution of intersecting cracks due to the cyclic loading. Some shear cracks spread throughout the entire height of the solid RC infill walls. However, the quantity of third-story shear cracks was much greater than that of the first-story, because the lateral load directly transferred from the top loading beam to the third-story solid RC infill wall. There were still no obvious signs of yielding on the surrounding steel frame. Figure 7 illustrates the process by which cracks develop in the RC infill walls under the different loading levels.

At the displacement control stage during the loading group of 0.5–1.0% overall drift ratio, some new shear cracks continued to occur and extended across the entire solid RC infill walls in the first and third stories. At the end of the second-story slit walls, many more flexural cracks were produced and the maximum width of the flexural cracks was nearly 4 mm. However, most of these new cracks were formed at the first cycle of each displacement level, and only minor cracks developed in the consecutive cycles. Because of the opening and closing of flexural cracks, a slight crush occurred at the interface of these minor serious flexural cracks, as shown in Fig. 8a. A visible opening was observed at all of

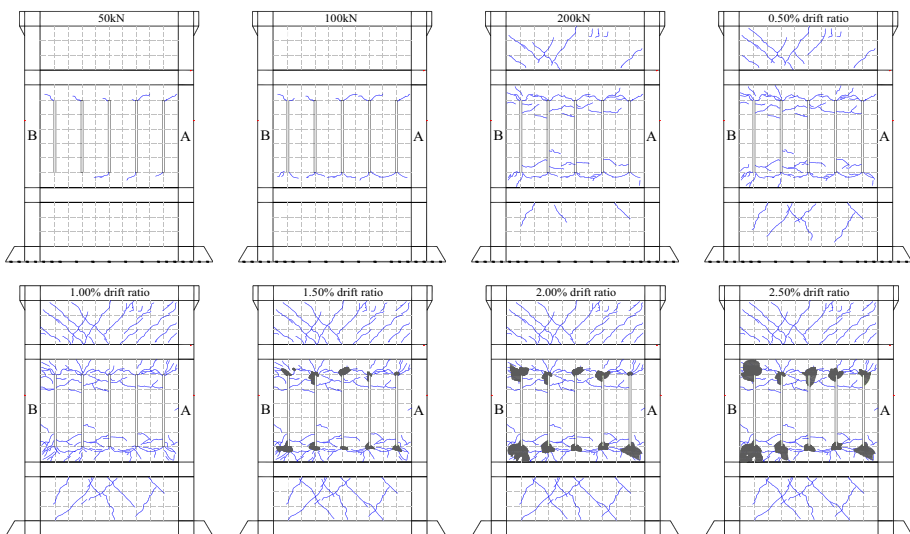


Fig. 7 Cracking and crushing patterns of the RC infill walls

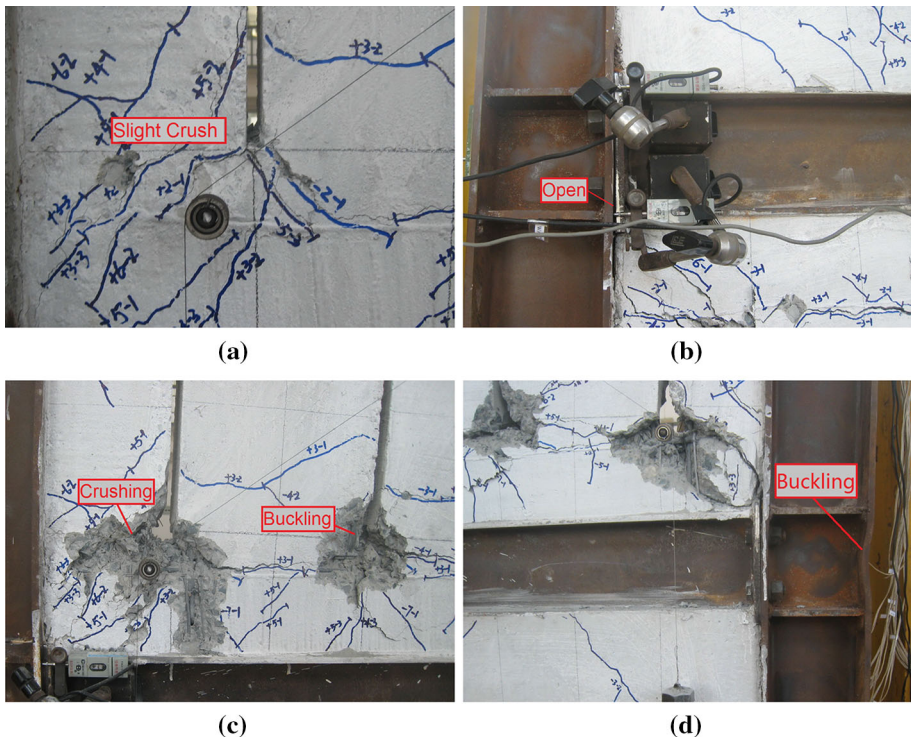


Fig. 8 Local failure photos of slit walls: **a** slight crush at the corners of slit walls; **b** opening of the flush end-plate connection; **c** severe crush at the ends of slit walls; **d** buckling at the outer flange of the steel column

the flush end plate connections, and some shear yielding lines appeared on the webs of the first- and second-story intermediate steel beam near the PR connections. The angle of the yielding lines was approximately $\pm 45^\circ$ under the cyclic loading. At the overall drift ratio of 1.00%, some yielding lines were observed on the webs of both column bases, and more yielding lines also appeared on the outer side flanges of both columns close to the base. During the loading group of 1.25–1.50% overall drift ratio, the specimen S-SLW reached its peak lateral strength of 385.44 and -379.87 kN in the push and pull loading direction, respectively. The maximum open distance of these four PR connections approached 1.6 mm, as illustrated in Fig. 8b. An obvious crush occurred at the corner of the slit wall adjacent to the B-column, and some concrete cover began to spall. The moderate pinching phenomenon visible on the hysteretic loops was a result of the cracking and crushing of the RC infill walls. During the loading group of 1.50–2.00% overall drift ratio, with the load continuing to increase, the crushing phenomenon was observed throughout all of the slit wall bases. The longitudinal bars inside the slit walls was exposed and buckled due to the spalling of the concrete cover, as shown in Fig. 8c. At the maximum load point of each loading cycle, the steel column at the second-story produced an obvious flexural deformation. Specially, both columns developed noticeable outward residual deformation resulting from the interactive compression between the columns and the RC infill walls, when the loading displacement returned to its initial position. During the loading group of 2.00–2.50% overall drift ratio, a noticeable local buckling of the outer flange of the steel

column was observed close to the connection panels of the second-story steel beam, as shown in Fig. 8d. The plastic hinges formed at the bases of the slit walls produced considerable rotation, which caused the concrete at the base of the slit walls to be severely crushed and spalled. At the 2.50% overall drift ratio, the test specimen was regarded as a failure because the lateral strength of specimen S-SLW had dropped to 80% of the peak load. Figure 9 shows the general failure photo of specimen S-SLW at the end of the test.

3.2 Hysteretic behavior

Figure 10 shows the relationship between the lateral load and the drift ratio of specimen S-SLW. It was clear that the drift ratios at the first and third stories were far less than that of the second story. The main reason was that the solid RC infill walls were adopted in the first and third stories, which significantly increased the lateral stiffness. Therefore, the hysteretic behavior of the second story with the slit RC infill walls was mainly analyzed hereafter. Generally, the specimen S-SLW exhibited a much greater full hysteretic loop than PSRCW with concealed vertical slits in the RC infill wall (Fig. 10e) or the solid RC infill wall (Fig. 10f). This phenomenon can be explained because the height-to-width of the slit wall was larger than 1, and the flexural deformation of the slit wall played an important role in improving the hysteretic behavior. At the same loading level, the subsequent second



Fig. 9 Failure photo of specimen S-SLW

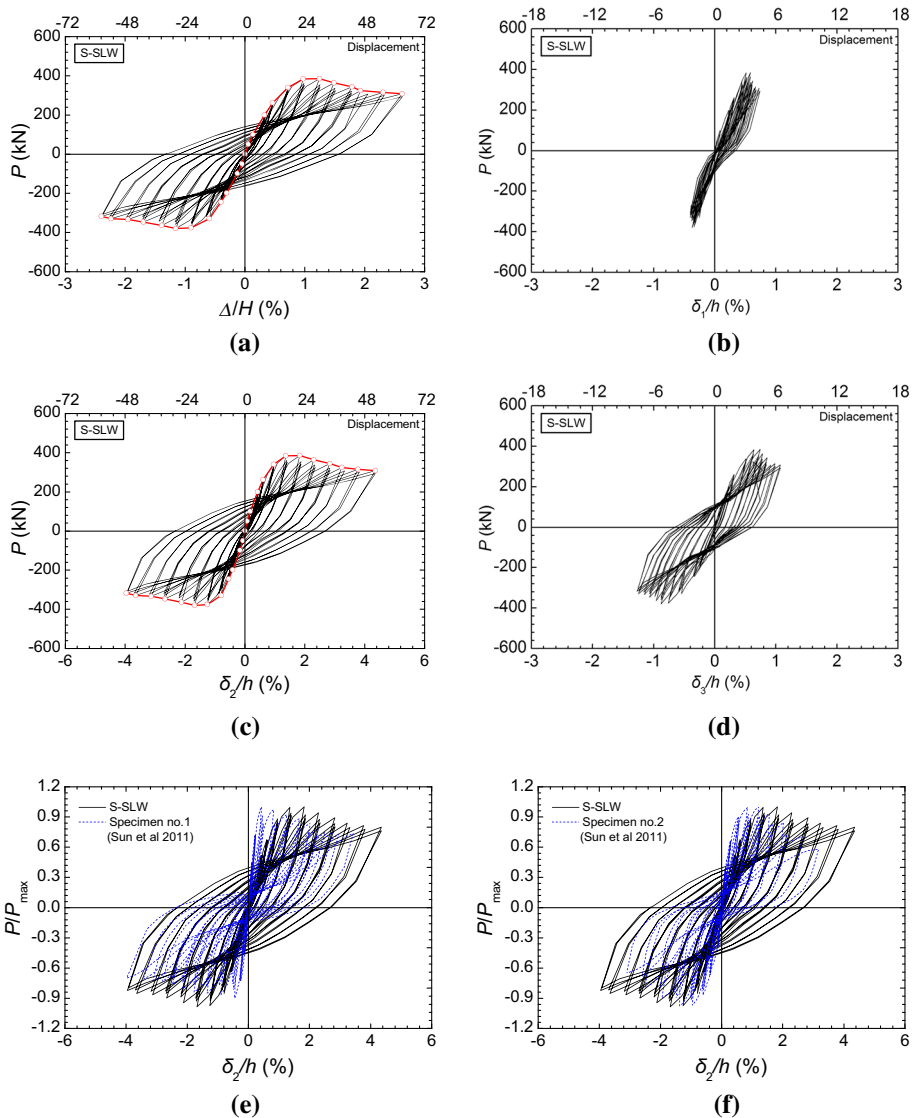


Fig. 10 Lateral load versus drift hysteretic curves: **a** total drift ratio of S-SLW; **b** first-story drift ratio of S-SLW; **c** second-story drift ratio of S-SLW; **d** third-story drift ratio of S-SLW; **e** second-story drift ratio of specimen no. 1 (Sun et al. 2011); **f** second-story drift ratio of specimen no. 2 (Sun et al. 2011)

and third hysteretic loops of specimen S-SLW exhibited slight strength and stiffness degradation compared with the first hysteretic loop. However, the lateral strength and stiffness of PSRCW with solid RC infill walls (Fig. 10f) degraded quickly at the same loading level. It was indicated that the flexural-dominated slit wall decreased the degradation at a slower rate than the shear-dominated solid RC infill wall. The slit walls dissipated considerable energy, and provided excellent deformability as well as ductility.

3.3 Strength, stiffness and ductility

The skeleton curves of the lateral load versus drift ratio for specimen S-SLW are shown in Fig. 11. The skeleton curves of specimen S-SLW exhibited an obvious “S” shape, which indicated that the test specimen underwent elastic, inelastic, and failure stages (Fig. 11a, b). The specimen S-SLW showed a slowly decreasing lateral carrying capacity after reaching its peak load, with the yielding of the longitudinal bars inside the slit walls and the concrete crushing located at the base of slit walls. The significant yielding point was determined according to the recommended method from FEMA 273. The yielding inter-story drift ratio of specimen S-SLW ranged from 0.63 to 0.72%, which was far larger than that of specimen no. 1 with its concealed vertical slit RC infill walls (Fig. 11c). When the lateral strength dropped to 85% of the peak load, the ultimate second inter-story drift ratio of specimen S-SLW had reached 3.77%, and the maximum inter-story ductility reached 5.24. The deformability and ductility of specimen S-SLW was improved significantly compared with the specimen no. 2 (Fig. 11d). The primary reason was that the deformation mode of the slit walls was controlled by a flexural-dominated pattern.

The average “peak to peak” stiffness, corresponding to the slope of the hysteretic loop using the line connecting the positive and negative peak points at the same loading level, was adopted to evaluate the lateral stiffness degradation of specimen S-SLW. Figure 12 shows the lateral stiffness degradation of specimen S-SLW under cyclic loading. The

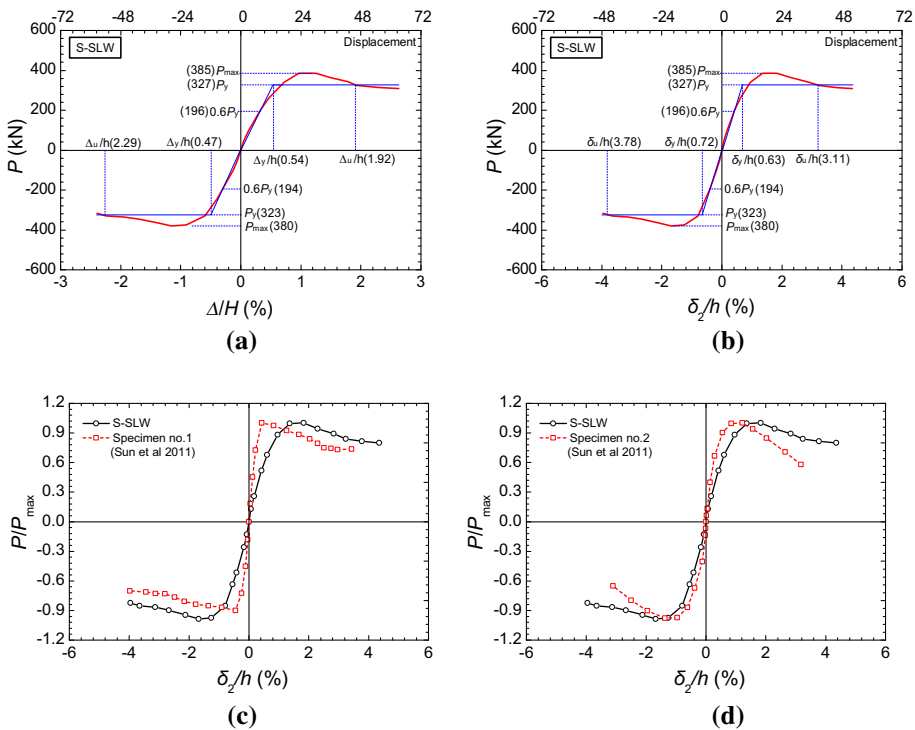


Fig. 11 Lateral load versus drift skeleton curves: **a** top drift ratio of S-SLW; **b** second inter-story drift ratio of S-SLW; **c** second-story drift ratio of specimen no. 1 (Sun et al. 2011); **d** second-story drift ratio of specimen no. 2 (Sun et al. 2011)

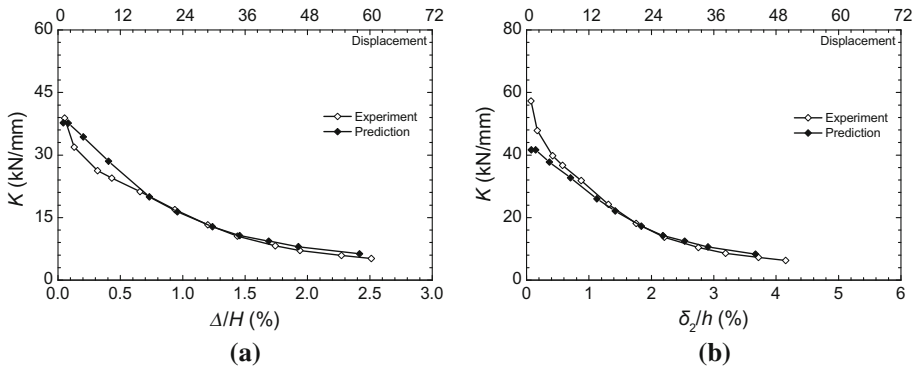


Fig. 12 Stiffness degradation: **a** top drift ratio; **b** second inter-story drift ratio

employment of slit walls can provide considerable lateral stiffness to resist wind or earthquake. During the general loading process, the lateral stiffness of specimen S-SLW deteriorated slowly without any abrupt change.

The test results, including the cracking drift ratio and cracking load, yielding drift ratio and yielding load, peak drift ratio and peak load, failure drift ratio and failure load, and ductility (μ_u) as well as cumulative ductility (μ_c), are provided in Table 2. The cumulative ductility, μ_c , is meant to provide a rough qualitative evaluation on the structural cumulative plastic deformation capacity (Teran-Gilmore and Bahena-Arredondo 2008). This indicator is equal to the sum of the residual displacements under all the hysteretic loops normalized by the yielding displacement (δ_y), which can be expressed as

$$\mu_c = \frac{2 \sum \delta_r}{\delta_y} \tag{1}$$

where δ_r is the residual displacement after each hysteretic cycle and δ_y is the significant yielding displacement.

From Table 2, the ultimate failure drift ratio ranged from 3.114 to 3.778% and the ductility for specimen S-SLW ranged from 4.94 to 5.24. The test results indicated that specimen S-SLW had excellent deformability and exhibited a ductile failure mode. The inter-story drift ratio, i.e., 0.07%, can be adopted as the cracking drift ratio limit for controlling the elastic response of specimen S-SLW, and avoiding the production of excessive cracks in specimen S-SLW resulting in a decrease in endurance under normal work conditions. The cumulative ductility was approximately equal to 42 in one loading direction. This parameter can be used to evaluate the structural cumulative damage, especially when the building was subjected to an earthquake with a distant fault.

3.4 Energy dissipation capacity

Figure 13 shows the cumulative dissipated energy and equivalent viscous damping ratio (ξ_{eq}) as a function of the second-story drift ratio. With the increase in lateral load, the cumulative hysteretic energy, E_h , tended to increase, indicating that more cumulative hysteretic energy was dissipated by the slit walls and the surrounding steel frame. The equivalent viscous damping, ξ_{eq} , is a more reasonable parameter to evaluate the structural hysteretic behavior. The equivalent viscous damping ratio of specimen S-SLW reached

Table 2 Test results of specimen S-SLW

Specimen	Loading direction	δ_c/h (%)	P_{cr} (kN)	δ_y/h (%)	P_y (kN)	δ_m/h (%)	P_m (kN)	δ_u/h (%)	P_u (kN)	μ_u	μ_c
S-SLW	Push	0.073	50	0.631	273.7	1.828	385	3.114	327.3	4.94	43.34
	Pull	- 0.071	- 50	- 0.721	- 295.6	- 1.683	- 380	- 3.778	- 323.0	5.24	42.06

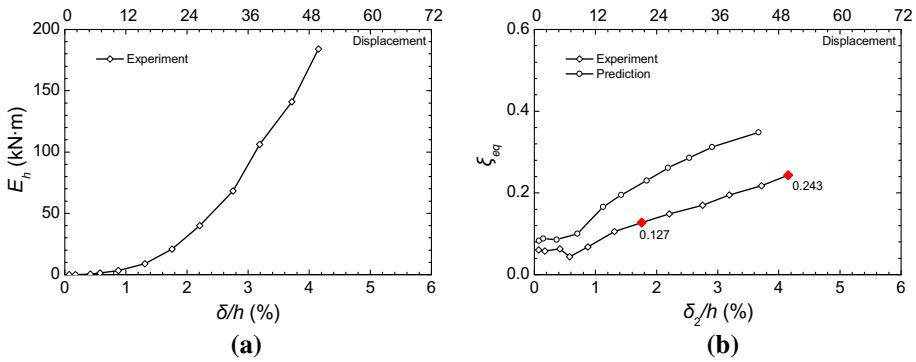


Fig. 13 Energy dissipation capacity of second story: **a** cumulative hysteretic energy; **b** equivalent viscous damping ratio

0.127 and 0.243 at peak and ultimate load, respectively. This indicated that specimen S-SLW developed a much fuller hysteretic curve and produced more plastic deformation with the increase in lateral load.

3.5 Lateral shear distribution in the PSRCW with vertical slits

In the composite PSRCW with vertical slits, the majority of lateral shear was sustained by the slit walls. However, to determine the percentage of lateral shear between the steel frame and the slit walls at various loading stages, the strains, including strain gages and rosettes mounted on key locations on the steel column, were recorded to compute this part of the lateral shear resisted by the steel frame. Figure 14 depicts the lateral shear resisted by the slit walls at the top and bottom interface of the second story. As seen from Fig. 14, at the initial loading stage, the slit walls carried approximately 85% of the total lateral shear, which was transferred from the steel beam to the slit walls through the shear connectors placed along the beam-wall interface. With the continued increase of the lateral load, the slit walls cracked and gradually formed plastic hinges at both ends. However, compared with the slit walls, the surrounding steel frame was damaged only slightly. Thus, the percentage resisted by the slit walls began to decrease, and the hysteretic curve exhibited a clear descending tendency. From the measured results, whether at the push or

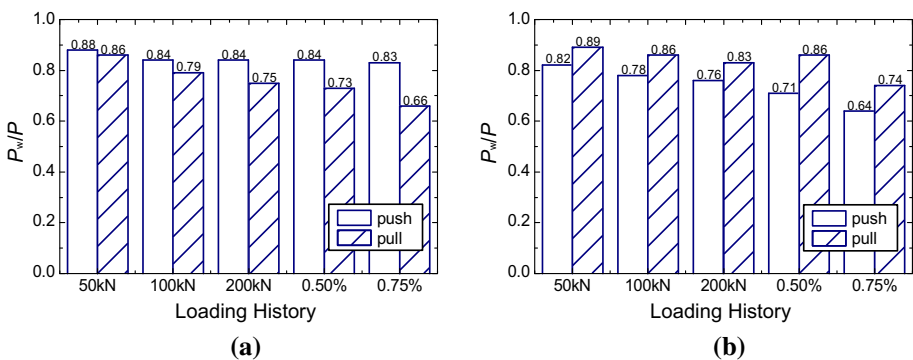


Fig. 14 Lateral shear resisted by the slit walls of the second story: **a** top interface; **b** bottom interface

pull loading direction, the slit walls almost sustained similar lateral shear at the same loading stage. Generally, at the design stage, the 80% lateral shear can be used to design the slit walls.

3.6 Behavior of flush end plate connections

In PSRCW with a slit wall system, the flush end plate connection was utilized to enhance the rotation capacity of beam-to-column connection. To monitor the actual mechanical behavior of PR connections used in specimen S-SLW, two LVDTs were attached on each PR connection. Figure 15 illustrates the lateral shear versus rotation relationship of the flush end plate connection adjacent to B-column. During the general loading stage, all of the PR connections did not produce a fracture failure. Because of the use of slit walls, the lateral stiffness of specimen S-SLW was enhanced significantly, and the rotation capacity demand on the beam-to-column connection was reduced. As shown in Fig. 15, the unsymmetrical hysteretic curves of the PR connections were obtained. The primary reason was that the employment of solid RC infill walls at the top and bottom story resulted in a different restraining influence on the flush end plate connection. According to the measured data, the maximum rotation of PR connections adjacent to B-column was 0.022 rad.

4 Numerical analysis

4.1 Simplified wall-column fiber model

The finite element method (FEM) can be used to simulate the mechanical behavior of a complex structure subjected to wind or earthquake. However, in some cases the analytical results do not provide enough precision compared with test results due to the restriction of the material cyclic constitutive relationship. In addition, the refined micro FEM requires a greater level of effort by the designer. Therefore, the designer generally requires a simplified method to obtain the available computing resources. As a practical analysis of a model of PSRCW with vertical slits, the macro wall-column model has been proposed by Mi (2010). During the test, the slit walls deform as a series of parallel flexural columns, as shown in Fig. 16. In the general deformation of PSRCW with vertical slits, the flexural

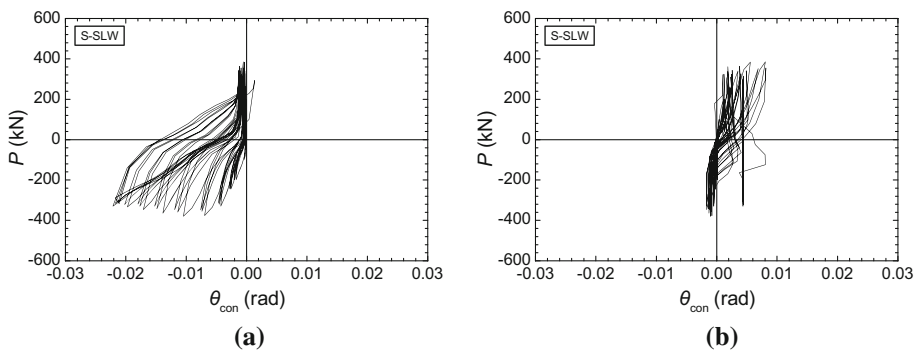


Fig. 15 Hysteretic curves of PR connections connected with B column: **a** top PR connection; **b** bottom PR connection

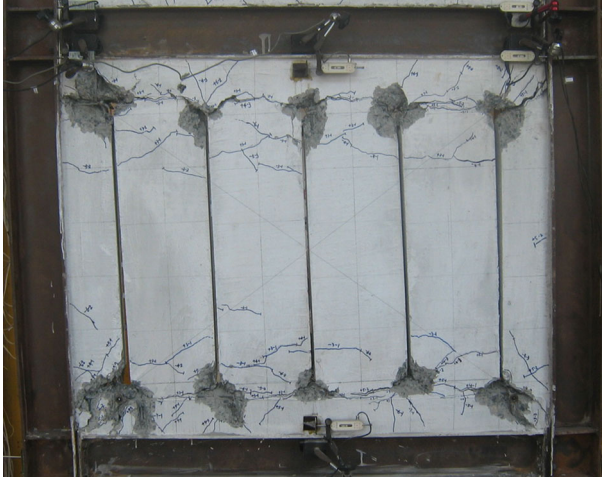


Fig. 16 Deformation feature of slit walls

deformation accounts for the majority and the shear deformation of the slit walls can be neglected. In this study, based on the original wall-column model, the simplified wall-column fiber model has been used to simulate the hysteretic behavior for PSRCW with vertical slits.

In the macro wall-column fiber model, the lateral story shear is resisted through the bending action of slit walls, which can be simulated as many discrete, fixed-ended columns using the fiber elements. In the actual slit walls, to anchor the longitudinal bars inside slit walls and transfer the lateral shear from the steel beam to the RC infill wall, the top and bottom parts known as concealed concrete beams are employed. Additionally, the concealed concrete beam has yet another function to avoid the RC infill wall splitting failure resulting from the shear connectors welded on the steel beam due to the limited thickness of the RC infill wall. Specifically, during the test the concealed concrete beams provide significantly large shear stiffness, producing small shear deformation. Therefore, in the macro wall-column fiber model, for simplicity, the concrete concealed beams are simulated as rigid ribs, and the intermediate steel beam can be simulated as a rigid beam for the contribution of the concrete concealed beam. Figure 17 shows the plane simplified macro wall-column fiber model used for the analysis of specimen S-SLW. In this simplified macro model, the fiber beam element is used to simulate the main components, including steel columns, steel beams, concealed concrete beams, and slit walls. The first- and third-story solid RC infill wall is modeled as a plane fiber shell element. The rotation spring element is adopted to simulate the flush end plate connection.

The following equation (Wang and Hsu 2001) is adopted for the stress–strain envelope relationship of concrete in the compressive and tensile stage.

$$\sigma = f_{ck} \left[2 \left(\frac{\varepsilon}{\varepsilon_0} \right) - \left(\frac{\varepsilon}{\varepsilon_0} \right)^2 \right] \quad \varepsilon/\varepsilon_0 \leq 1 \quad (2)$$

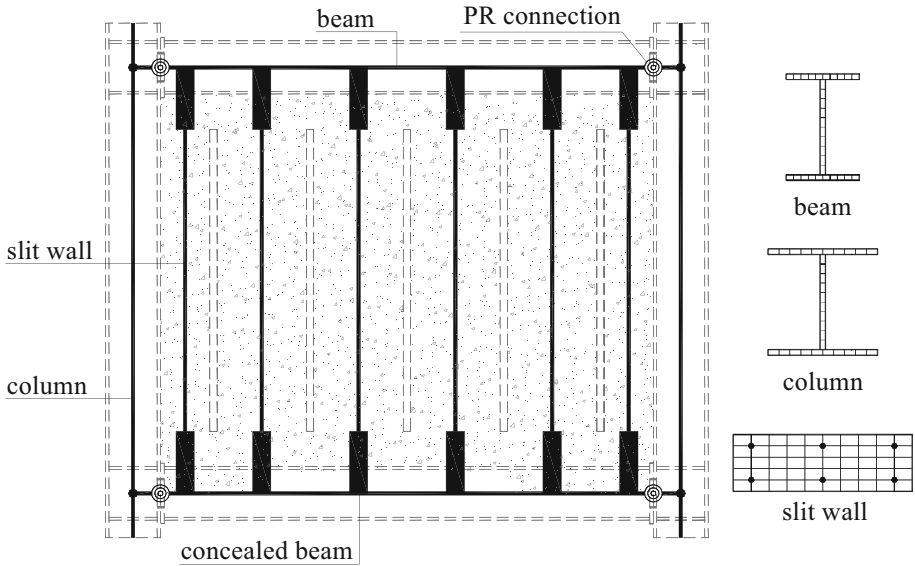


Fig. 17 Simplified macro wall-column fiber model of PSRCW with vertical slits

$$\sigma = f_{ck} \left[1 - \left(\frac{\varepsilon/\varepsilon_0 - 1}{3} \right)^2 \right] \quad \varepsilon/\varepsilon_0 > 1 \tag{3}$$

$$\sigma = 0.2f_{ck} \quad \varepsilon \geq 3.68\varepsilon_0 \tag{4}$$

where σ is the stress of concrete; ε is the strain of concrete; f_{ck} is the compressive strength of the concrete cylinder; and ε_0 is the peak strain of concrete, which can be taken to be 0.002.

$$\sigma = E_c \varepsilon \quad \varepsilon \leq \varepsilon_{cr} \tag{5}$$

$$\sigma = f_{tk} \quad \varepsilon \geq \varepsilon_{cr} \tag{6}$$

where E_c is the elastic modulus of concrete and f_{tk} is the tensile stress of concrete.

Figure 18 shows the simplified cyclic stress versus strain relationship of concrete used in the concrete fiber element.

The simplified bilinear stress–strain relationship of steel or steel bar is adopted in the macro wall-column fiber model, as shown in Fig. 19. The kinematics of the hardening plastic hysteretic model is used to reflect the Bauschinger effect, and the post-stiffness ratio is taken as 0.02.

The component method recommended by the EC3 specification (2005) is used to compute the rotation stiffness and ultimate moment capacity of the flush end plate connection. The rotation stiffness of the flush end plate connection can be calculated in the following form:

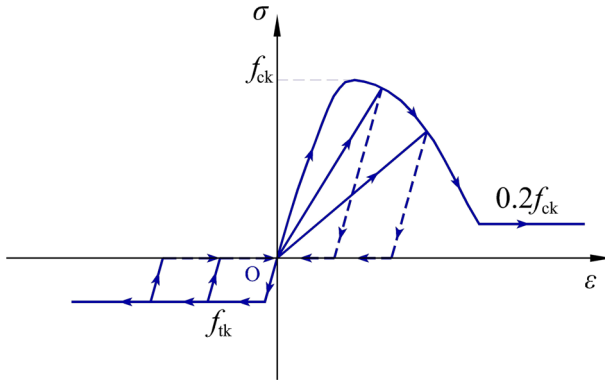
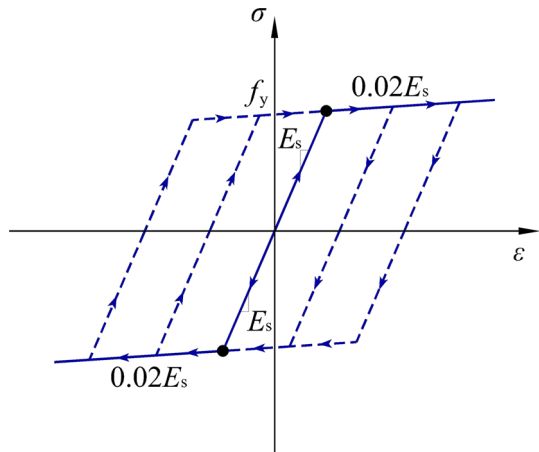


Fig. 18 Simplified stress versus strain curve of concrete under cyclic loading

Fig. 19 Stress versus strain curve of steel under cyclic loading



$$K_0 = \frac{E_s z_{eq}^2}{\mu \sum_i \frac{1}{k_i}} \tag{7}$$

where K_0 is the initial rotation stiffness of the flush end plate connection; z_{eq} is the equivalent lever arm; E_s is the elastic modulus of steel; k_i is the stiffness coefficient for the basic joint component i ; and μ is the stiffness ratio.

In calculating K_0 , the contributions, including the column flange in bending, end-plate in bending, flange cleat in bending, and high-strength bolts in tension, are considered. When stiffened ribs are used inside the steel column corresponding to the location of the steel beam flange, the effect of the column web panel in shear, compression, and tension can be neglected.

The component method proposed by the EC3 specification (2005) can also be used to compute the ultimate moment resistance capacity of the flush end plate connection, which can be determined as:

$$M_{PR} = \sum_r F_{t,PR,r} h_r \tag{8}$$

$$F_{t,PR,r} = \min \left\{ \frac{F_{s,wc,PR}}{\beta}, F_{t,wc,PR}, F_{t,fc,PR}, F_{t,ep,PR}, F_{t,wb,PR} \right\} \tag{9}$$

where M_{PR} is the moment resistance capacity of the flush end plate connection without considering the axial force; r is the row number of bolts; and h_r is the distance from row r to the center of compression. $F_{t,PR,r}$ is the effective tension resistance of bolt-row r . The effective tension resistance $F_{t,PR,r}$ of bolt-row r , taken as an individual bolt row, should be taken as the smallest value of the tension resistance for an individual bolt row of the following basic components, including the column web in shear ($F_{s,wc,PR}$), the column web in tension ($F_{t,wc,PR}$), the column flange in bending ($F_{t,fc,PR}$), the end-plate in bending ($F_{t,ep,PR}$), and the beam web in tension ($F_{t,wb,PR}$). β is the transformation parameter.

In addition, the ultimate moment resistance capacity of the flush end plate connection used in PSRCW with vertical slits should take into account the effect of the axial force in the steel beam. The axial force results from the difference in the lateral shear of adjacent two-story RC infill walls (Fig. 20), which can be computed in the following expression.

$$T_{PR,i} = \frac{2 \sum (M_{slit,i} - M_{slit,i+1})}{h_{s,hinge}} \tag{10}$$

where T_{PR} is the tensile force sustained by the PR connection; M_{slit} is the plastic moment resisting capacity of a single slit wall; and $h_{s,hinge}$ is the clear distance between both plastic hinges in a single slit wall.

Tong (2001) proposed the moment-tensile interaction equation to reflect the influence of axial tension, as follows

$$\left(\frac{M_{y,PR-t}}{M_{y,PR}} \right)^{1.75} + \left(\frac{T_{PR}}{T_{y,PR}} \right)^{1.75} = 1 \tag{11}$$

where $M_{y,PR}$ and $T_{y,PR}$ are the yield moment and tensile capacity of the PR connection, respectively.

For simplicity, the tri-linear moment versus rotation relationship curve is also adopted to analyze the hysteretic behavior of the flush end plate connection, as shown in Fig. 21. The ultimate moment (M_u) of the PR connection can be computed through replacing the yield strength (f_y) with the ultimate strength (f_u) of steel. The rotation stiffness ratio at the post-yielding stage of the PR connection is taken as 0.35. According to the above proposed approach, the yielding moment (M_y) and ultimate moment (M_u) of the PR connection

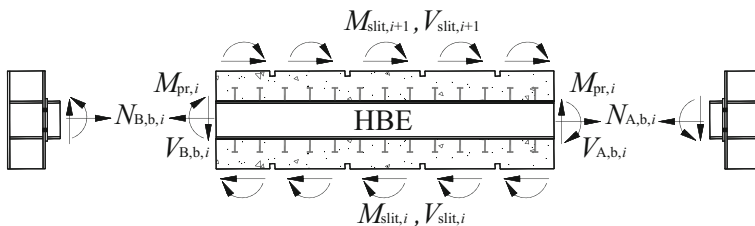
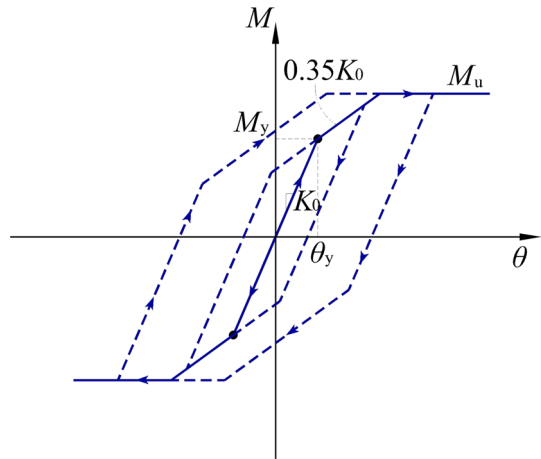


Fig. 20 Axial force sustained by a PR connection

Fig. 21 Moment versus rotation curve of a PR connection under cyclic loading



considering the effect of the axial force are 18.54 and 25.73 kN m, respectively. Additionally, the initial rotation stiffness of the PR connection is 7374.1 kN m/rad.

4.2 Verification of the simplified wall-column fiber model

To verify the accuracy of the FEM simulation using the simplified wall-column fiber model of PSRCW with vertical slits subjected to cyclic loading, cyclic analysis of specimen S-SLW tested in this paper was performed, and the finite element program PERFORM 3D (CSI 2011) was selected for conducting the cyclic analysis on the global behavior of the PSRCW with vertical slits. The surrounding steel column, steel beam as well as slit wall are simulated as fiber beam elements. The intermediate steel beam between the PR connections was regarded as a rigid beam due to the effect of a concealed concrete beam located in the anchor region of the slit walls. The flush end plate connection was modeled with the nonlinear rotation spring element. In addition, considering the limit influence on the general behavior of specimen S-SLW from the first- and third-story solid RC infill walls, the elastic plane shell element was adopted. The second-order geometry nonlinearity was also considered. Figure 22 illustrates the simplified wall-column fiber model of specimen S-SLW.

Figure 23 shows the predictions and test results for specimen S-SLW. As shown in Fig. 23, the maximum lateral load-carrying capacity predicted by the macro fiber model were + 385.72 and – 393.74 kN in the push and pull loading directions, respectively, which were similar to the + 385.44 and – 379.87 kN of the test results. The simplified macro fiber model successfully predicted the maximum lateral load-carrying capacity of specimen S-SLW. From Fig. 12, the general initial lateral stiffness was similar to the test results. However, the predicted initial lateral stiffness of the second story was underestimated by approximately 38% compared with the test results. As the load increased, the discrepancy between the test results and predictions gradually decreased. Figure 13 also showed that the predicted equivalent viscous damping ratio was larger than that of the test results. This indicated that the hysteretic curve obtained from numerical simulation was fuller than the test hysteretic curve. The discrepancy in the equivalent viscous damping ratio between the test results and predictions tended to increase with increasing lateral load.

Fig. 22 Simplified wall-column fiber model for specimen S-SLW

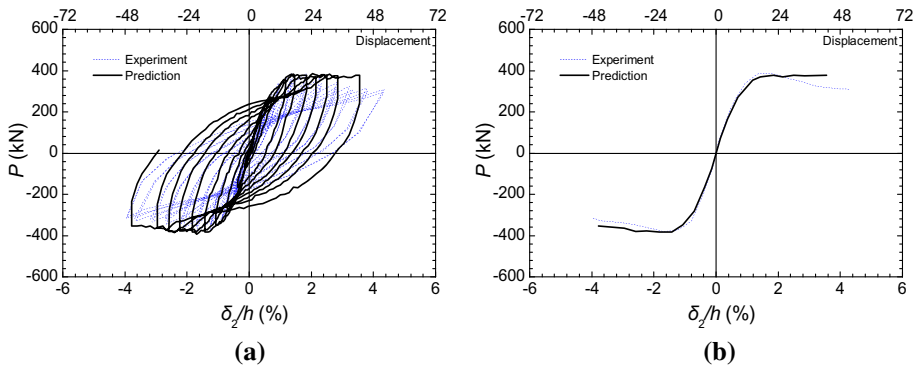
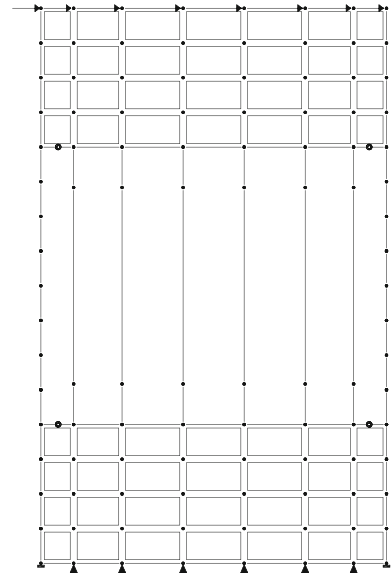


Fig. 23 Predictions for specimen S-SLW: **a** hysteretic curves; **b** skeleton curves

As a result, this simplified macro wall-column fiber model was able to capture the primary mechanical behavior of PSRCW with vertical slits with an acceptable accuracy.

4.3 Parametric study

Parametric studies were performed by using this simplified macro wall-column fiber model to investigate the effect of various factors on the hysteretic behavior of PSRCW with vertical slits. A single-story, one-bay PSRCW with vertical slits was redesigned and named the BASE specimen. The main reason for removing the top and bottom half-story is that the hysteretic behavior of the solid RC infill wall is difficult to simulate using the current concrete cyclic constitutive relationship. The span of the BASE specimen is 1500 mm, and the height is 1200 mm. The surrounding steel column is H150 × 150 × 7 × 10, and the top beam is H150 × 100 × 6 × 9. The details and dimensions of the slit walls of the

BASE specimen in the parametric study are the same as the second story of the test specimen S-SLW. The cubic concrete strength is taken as $f_{cu} = 30 \text{ N/mm}^2$. The yielding strengths of profile steel and steel bar are taken as $f_y = 235 \text{ N/mm}^2$ and $f_y = 335 \text{ N/mm}^2$, respectively. In all calculation models, the following parameters are investigated:

1. Type of beam-to-column connection: Pinned, Partially restrained (PR), and Fully restrained (FR) connection;
2. Height-to-width ratio of slit wall: $\alpha = 1.5, 3, \text{ and } 5$;
3. Concrete strength of slit wall: $f_{cu} = 20, 30, \text{ and } 40 \text{ N/mm}^2$;
4. Steel bar ratio of slit wall: $\rho = 0.85, 1.50, \text{ and } 3.40\%$.

In the parametric study, the relative mechanical properties of the PR connection used in the PSRCW with vertical slits are taken as the same as the S-SLW of the test specimen.

4.3.1 Effect of beam-to-column connection type

Figure 24 shows that it is obvious that the changing of the beam-to-column connection type significantly affects the shape of hysteretic loop, lateral strength, and initial stiffness of PSRCW with vertical slits. When the beam-to-column connection changing from pinned to PR, and FR connection, the maximum lateral load-carrying capacity of PSRCW with vertical slits increases from 253.6 to 301.25, and 325.5 kN, and the initial lateral stiffness is also enhanced from 36.25 to 45.45, and 54.09 kN/mm. In addition, the fuller hysteretic

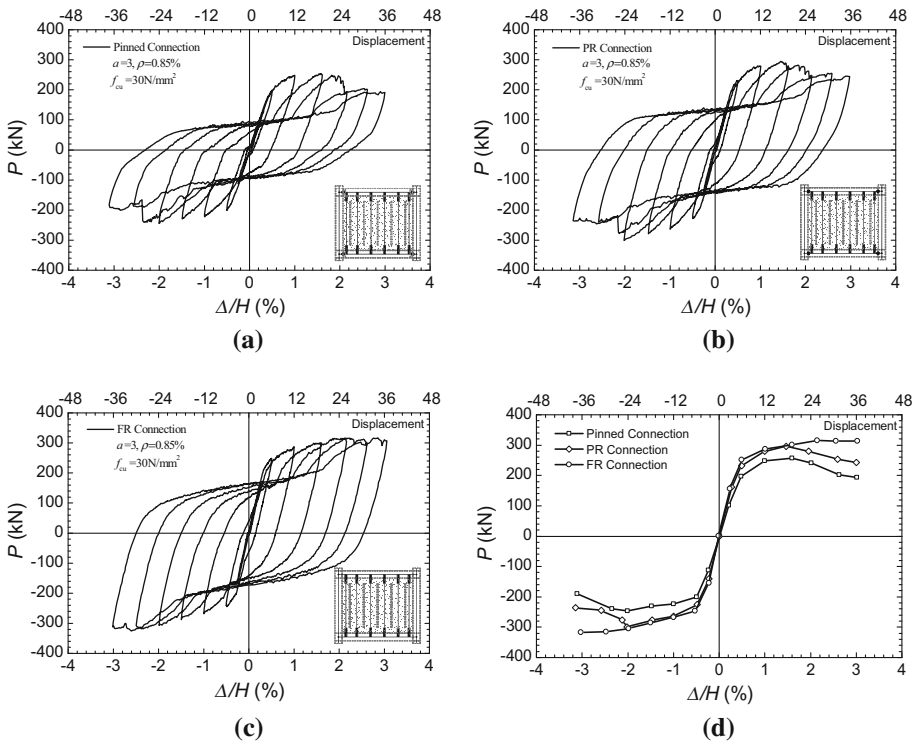


Fig. 24 P-Δ curves of series specimens considering the effect of the beam-to-column connection type: **a** pinned connection; **b** PR connection; **c** FR connection; **d** Skeleton curves

loop of PSRCW with vertical slits is also obtained, as the PR or FR beam-to-column connection is used in the surrounding steel frame. This phenomenon can be explained in that the mechanical behavior of PSRCW with vertical slits consists of two parts, including the surrounding steel frame and the internal slit walls. When the surrounding steel frame is strengthened, it will play a more important role in increasing the lateral load-carrying capacity and lateral stiffness. Additionally, the steel frame possesses a much greater hysteretic loop, while the slit walls have much more of a pinching hysteretic loop. Therefore, the hysteretic loops of PSRCW with vertical slits develop considerably full due to the employment of much stronger surrounding steel frame.

4.3.2 Effect of height-to-width ratio of slit wall

Figure 25 shows the effect of the height-to-width ratio of the slit wall on the hysteretic behavior and lateral strength of PSRCW with vertical slits. In these analytical examples, the height-to-width ratios are taken as 1.5, 3, and 5, while the overall quantities of steel bars inside slit RC infill wall still remain the same. Only the width of the slit wall changes. As seen from Fig. 25, when the height-to-width ratio increases from 1.5 to 3 and then to 5, the lateral load-carrying capacity of the PSRCW with vertical slits decreases by 14.4 and 44.6%, respectively. Specifically, when the height-to-width ratio increases to 5, the lateral load-carrying capacity drops quite quickly. However, the hysteretic loop shape gradually becomes fuller. This is because the narrow slit wall provides much less flexural resisting

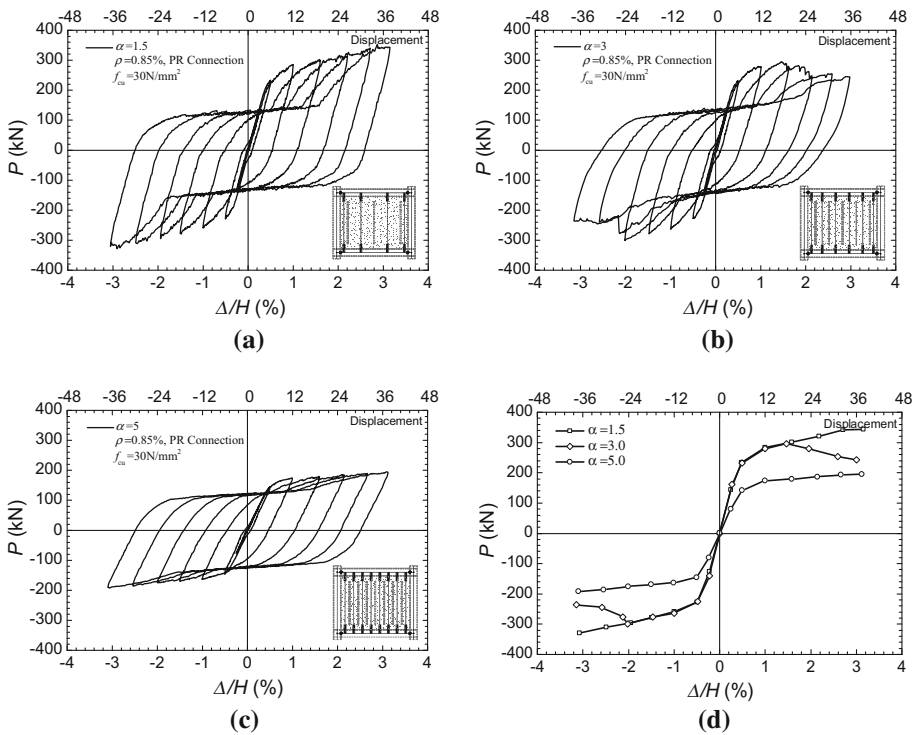


Fig. 25 *P*- Δ curves of a series of specimens considering the effect of the height-to-width ratio of a slit wall: **a** $\alpha = 1.5$; **b** $\alpha = 3$; **c** $\alpha = 5$; **d** skeleton curves

capacity, and the surrounding steel frame with excellent hysteretic behavior plays a more important role in this composite structural system.

4.3.3 Effect of concrete strength

Figure 26 shows the effect of concrete strength on the hysteretic behavior of PSRCW with vertical slits. It is evident from the results presented in Fig. 26 that the concrete strength of the slit wall plays an important effect on the lateral load-carrying capacity except for the initial lateral stiffness and hysteretic behavior. All of the PSRCW structures exhibit a similar hysteretic loop shape, i.e., still display the obvious pinning hysteretic feature. Although the elastic modulus of concrete is enhanced resulting from the increase in concrete strength, the flexural stiffness of the slit wall does not exhibit a noticeable improvement. This indicates that the increment of the concrete elastic modulus due to the change in concrete strength is quite small, and this effect on lateral stiffness of PSRCW with vertical slits can be ignored. As the concrete strength increases from $f_{cu} = 20$ –30, and 40 N/mm^2 , the maximum lateral load-carrying capacity of a PSRCW with vertical slits reaches 258.99, 301.25, and 329.98 kN, respectively.

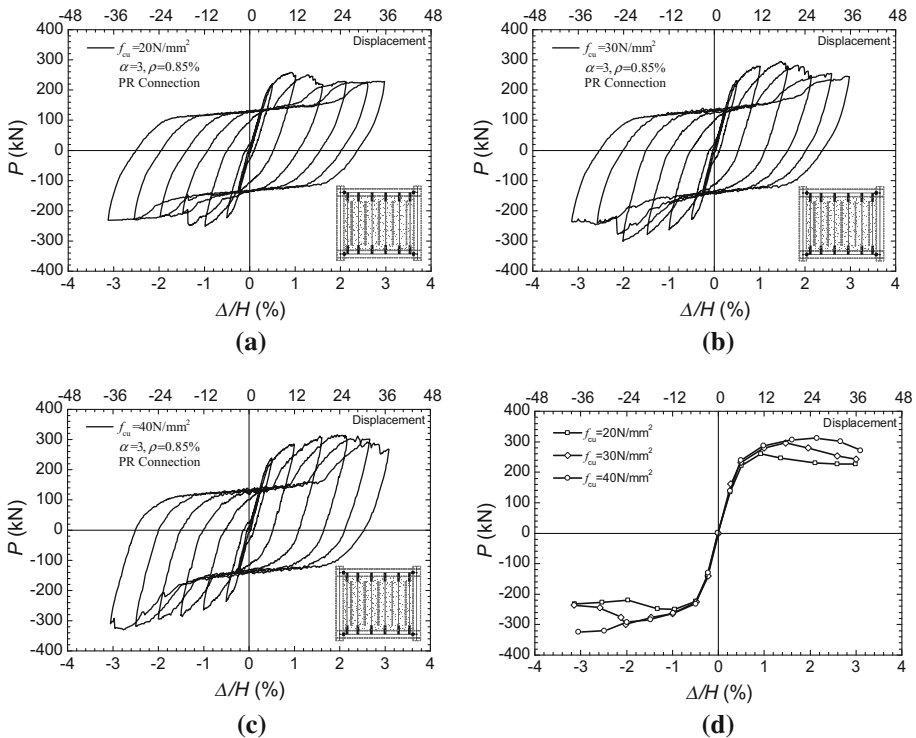


Fig. 26 P - Δ curves of a series of specimens, considering the effects of concrete strength: **a** $f_{cu} = 20 \text{ N/mm}^2$; **b** $f_{cu} = 30 \text{ N/mm}^2$; **c** $f_{cu} = 40 \text{ N/mm}^2$; **d** Skeleton curves

4.3.4 Effect of steel bar ratio

The effect of changing the steel bar ratio inside slit walls on the hysteretic behavior and lateral load-carrying capacity is illustrated in Fig. 27. Three different steel bar ratios $\rho = 0.85, 1.50,$ and 3.40% are selected herein, corresponding to steel bar with diameters of 6, 8, and 12 mm, respectively. It can be seen from Fig. 27, with the increase in the steel bar ratio, the maximum lateral load-carrying capacity tends to increase. When the steel bar ratio increases from 0.85 to 1.50, and 3.40%, the maximum lateral load-carrying capacity of the PSRCW with vertical slits increases by 8.1 and 16.9%, respectively. Specifically, with the increase in the steel bar ratio, the post-peak behavior of the PSRCW with vertical slits is significantly improved. The lateral load-carrying capacity shows an increasing trend due to the contribution of the steel bars. However, the steel bar ratio produces no clear effect on the initial lateral stiffness and hysteretic behavior of the PSRCW with vertical slits.

5 Conclusions

In this paper, the hysteretic behavior of composite partially restrained steel frame-reinforced concrete infill walls with vertical slits was investigated. A three-story, one-bay PSRCW at the one-third-scale with a sub-assembly of vertical slits was tested under

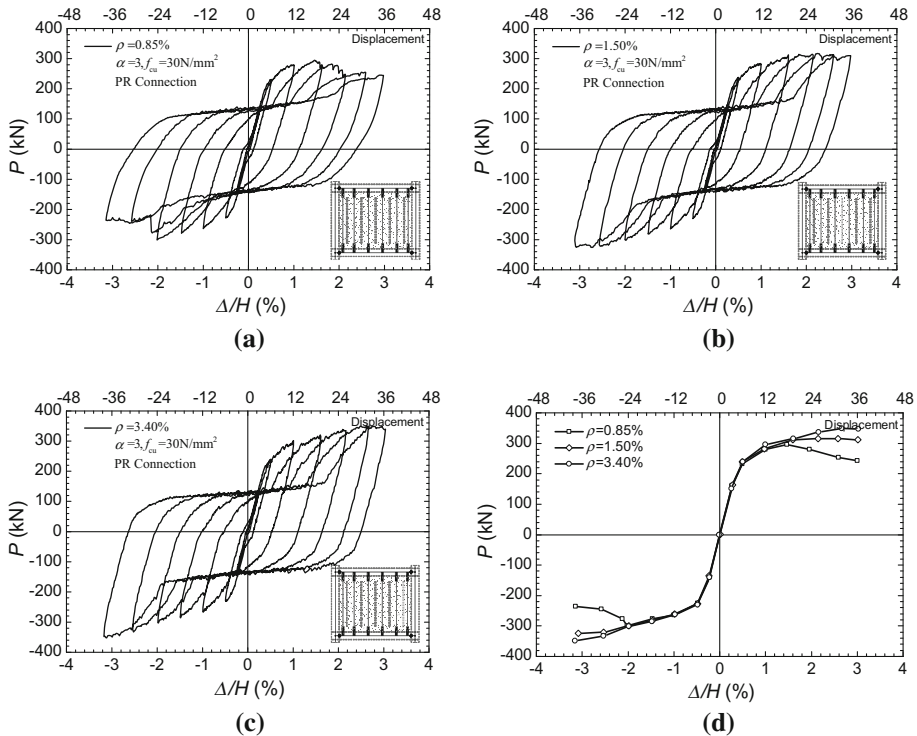


Fig. 27 P - Δ curves of the series specimen considering the effect of the steel bar ratio: **a** $\rho = 0.85\%$; **b** $\rho = 1.50\%$; **c** $\rho = 3.40\%$; **d** skeleton curves

cyclic lateral loading. The simplified wall-column fiber model for simulating its hysteretic behavior was validated based on the current test results. In addition, parametric studies were also performed based on the wall-column fiber model to investigate their influence on the hysteretic behavior of PSRCW with vertical slits. The following conclusions can be drawn from this investigation:

1. The PSRCW with vertical slits showed superior deformability and ductility capacity, excellent energy dissipation capacity, and good initial stiffness as well as lateral load-carrying capacity. The PSRCW with vertical slits obtained the ideal progressive ductile failure mode, and exhibited flexure-dominated behavior. The story ductility ratio of PSRCW with vertical slits was in the range of 4.94–5.24, and the cumulative ductility ratio was approximately 42 in a single loading direction.
2. In the slit walls, the majority of flexural cracks developed and focused on both ends of the slit walls. The crack drift of the PSRCW with vertical slits was approximately 0.07%, and the ultimate failure drift ranged from 3.114 to 3.778%, which could be sufficient to prevent collapse.
3. In this composite structural system, the percentage of lateral shear sustained by slit walls was approximately 85% at the initial elastic stage. With the slit wall cracking and crushing, this percentage tended to decrease.
4. The employment of slit walls reduced the demand on the surrounding steel frame resulting from an earthquake, and avoided the fracture failure of the beam-to-column connection. The maximum rotation of the flush end plate connection was no more than 0.022 rad.
5. The macro wall-column fiber model was validated as a simplified method to simulate the hysteretic behavior of a PSRCW with vertical slits with an accepted precision.
6. The beam-to-column connection type significantly affects the hysteretic behavior, lateral strength, and initial stiffness of a PSRCW with vertical slits. With the beam-to-column connection changing from pinned to PR and then to an FR connection, the maximum later load-carrying capacity and initial lateral stiffness exhibits a tendency to increase. As the height-to-width ratio of the slit wall increases, the lateral strength and initial lateral stiffness of the PSRCW with vertical slits both decrease, but the hysteretic loop develops a fuller shape. With an increase in the concrete strength and steel bar ratio of the slit wall, the lateral strength increases. The concrete strength and steel bar ratio do not produce a clear effect on the hysteretic behavior and initial stiffness.

Acknowledgements The research reported here was financially supported by the National Natural Science Foundation of China (Grant No. 51108292) and the Natural Science Foundation of the Jiangsu Higher Education Institutions of China (Grant No. 17KJA560003). The writers wish to express their sincere gratitude to these sponsors.

References

- Cao ZG, Du P, Fan F et al (2017) Cyclic testing and parametric analyses of the fabricated steel frames infilled with autoclaved aerated concrete panels. *Adv Struct Eng* 20(4):629–640
- CSI (2011) *PERFORM-3D V5: nonlinear analysis and performance assessment for 3D structures: user manual*. Computer and Structures, Inc., 1995 University Avenue, Berkeley, CA
- European Standard, EuroCode 3 (2005) *Design of steel structures-part 1-8: design of joints*. EN 1993-1-8

- Hajjar JF (2002) Composite steel and concrete structural systems for seismic engineering. *J Constr Steel Res* 58(5–8):703–723
- Hou HT, Chou CC, Zhou J et al (2016) Cyclic tests of steel frames with composite lightweight infill walls. *Earthq Struct* 10(1):163–178
- Lian XF, Zou CY (1996) Test research on the working behavior of RC shear panels with vertical seams under low-cyclic loading. *J Harbin Univ Arch Eng* 29(1):31–36 (in Chinese)
- Liao FY, Han LH, Tao Z (2009) Seismic behaviour of circular CFST columns and RC shear wall mixed structures: experiments. *J Constr Steel Res* 65:1582–1596
- Liao FY, Han LH, Tao Z (2012) Performance of reinforced concrete shear walls with steel reinforced concrete boundary columns. *Eng Struct* 44:186–209
- Liauw TC, Kwan KH (1983) Plastic theory of non-integral infilled frames. *P I Civil Eng* 75:379–396
- Liauw TC, Kwan KH (1985) Static and cyclic behaviors of multistory infilled frames with different interface conditions. *J Sound Vib* 99(2):275–283
- Lignos DG, Moreno DM, Billington SL (2014) Seismic behavior of a coupled wall system with HPFRC material in critical regions. *J Struct Eng* 140(3):04013072
- Makino M (1985) Design of framed steel structures with infill reinforced concrete walls. In: Roeder CW (ed) *Composite and mixed construction*. ASCE, New York (NY), pp 279–287
- Mallick DV, Severn RT (1968) Dynamic characteristics of infilled frames. *P I Civil Eng* 39:261–287
- Mi XF (2010) Wall-column frame model of RC slit wall. *Eng Mech* 27(1):188–194 (in Chinese)
- Olsen EC, Billington SL (2011) Cyclic response of precast high-performance fiber-reinforced concrete infill panels. *ACI Struct J* 108(1):51–60
- Omori S, Toyama K, Cho T, Takahashi T (1966) Test on RC shear wall with slits. *Summaries of technical papers of annual meeting AIJ, Kanto, Japan*, pp 204–205
- Peng XT, Gu Q (2013) Seismic behavior analysis for composite structures of steel frame-reinforced concrete infill wall. *Struct Des Tall Spec* 22:831–846
- SAC joint venture (1997) Protocol for fabrication, inspection, testing, and documentation of beam-column connection tests and other experimental specimens. Report no. SAC joint venture, Sacramento, CA
- Sánchez-Olivares G, Tomás A (2013) Design of planar semi-rigid steel frames using genetic algorithms and component method. *J Constr Steel Res* 88:267–278
- Sun GH, He RQ, Gu Q, Fang YZ (2011) Cyclic behavior of partially-restrained steel frame with RC infill walls. *J Constr Steel Res* 67(12):1821–1834
- Teran-Gilmore A, Bahena-Arredondo N (2008) Cumulative ductility spectra for seismic design of ductile structures subjected to long duration motions: concept and theoretical background. *J Earthq Eng* 12(1):152–172
- Tong XD (2001) Seismic behavior of composite steel frame-reinforced concrete infill wall structural system. Ph.D. thesis, Department of Civil Engineering, University of Minnesota, Minnesota, USA
- Tong XD, Hajjar JF, Schultz AE, Shield CK (2005) Cyclic behavior of steel frame structures with composite reinforced concrete infill walls and partially-restrained connections. *J Constr Steel Res* 61(4):531–552
- Wang TJ, Hsu TTC (2001) Nonlinear finite element analysis of concrete structures using new constitutive models. *Comput Struct* 79:2781–2791
- Wang JF, Li BB, Li JC (2017) Experimental and analytical investigation of semi-rigid CFST frames with external SCWPs. *J Constr Steel Res* 128:289–304
- Wu HH, Zhou TH, Liao FF et al (2016) Seismic behavior of steel frames with replaceable reinforced concrete wall panels. *Steel Compos Struct* 22(5):1055–1071
- Zhao W, Tong GS, Yang QY (2012) Experimental study on seismic behavior of steel frame with prefabricated reinforced concrete infill slit shear walls. *J Build Struct* 33(7):140–146 (in Chinese)